Proceedings of the 2004 IEEE
International Conference on Robotics & Automation
New Orleans, LA • April 2004

Design of an Artificial Muscle Continuum Robot

Michael B. Pritts and Christopher D. Rahn
Department of Mechanical Engineering
The Pennsylvania State University
University Park, PA
cdrahn@psu.edu

Abstract— **This paper introduces a novel continuum manipulator consisting of two flexible sections connected by rigid base plates. Each section uses 6 – 8 opposing contracting and extending McKibben actuators to provide two-axis bending. The contracting/extending actuator pairs are sized and positioned to provide matched rotation and torque. The experimental manipulator generates large rotation (30 – 35 degrees per section and 50 degrees for the entire manipulator) and load capacity (25 lb vertical lift) at 60 psi. With a large strength to weight ratio, this manipulator also is highly flexible, simple to manufacture, and low cost.**

Keywords-Soft manipulator; McKibben actuator.

I. INTRODUCTION

Many animal appendages have little or no fixed skeletal structure. These organs, termed 'muscular-hydrostats' include elephant trunks, squid tentacles, and human tongues. With no rigid backbone to aid movement, a muscular-hydrostats' control relies on the elongation and contraction of constant-volume muscles [2]. Although their makeup would appear to put them at a disadvantage, these structures are uncommonly flexible and have high degrees of freedom.

Muscular-hydrostats have great flexibility and control so there is considerable interest in developing robots that mimic their functionality. These continuum robots have been designed using a variety of actuators, including pressurized polyurethane tubes [5] and cable systems [9,10].

Research into the morphology of muscular-hydrostats has led to greater understanding of their biomechanics. Extremity extension is achieved by decreasing the cross-sectional area of constant-volume longitudinal muscles (*e.g.* starfish feet [7]). Similarly, increasing the cross-sectional area of the muscles decreases length. The determining factor on the direction and magnitude of linear displacement distance has been found to be the initial wind angle of the fibers in the muscle. Contraction occurs when this angle, measured from the longitudinal axis of the muscle, is less than 54°44'. Expansion under pressure occurs when the mesh angle is above 54°44' [8]. Because of this behavior, pressure vessels and tubing are often reinforced using fibers with this critical angle.

This research was supported by NASA and DARPA

Robinson and Davies [4] defined three classifications of continuum robots based on the type of actuation employed: intrinsic, extrinsic, or a hybrid of the two. Intrinsic robots use actuators physically located in the robot, whereas extrinsic robots use remote actuation that is transferred to the robot via linkages. Robinson and Davies [4] further subdivided these classifications into planar, those having a single plane of bending, and spatial, those having the ability to bend in any direction perpendicular to their axis.

The objective of this research is to design an intrinsic spatial continuum robot modeled after muscular-hydrostats. In order to model the constant-volume muscles of muscular-hydrostats, McKibben artificial muscles are used as actuators. McKibben actuators can be constructed by covering an elastic tube, often latex, with a braided plastic mesh [3]. Much like movement in muscular-hydrostats, linear displacement of the actuator depends on the mesh angle of the plastic sheath. Using compressed air, these actuators can provide 20-30% strain with large force capacity for a contracting actuator with small wind angle [8]. The actuator extends for wind angles above 54°44'.

II. MANIPULATOR DESIGN

Figure 1 shows the manipulator design. The robot divides into two sections consisting of McKibben muscle actuators connected to rigid base plates at the end of each section. Air is supplied to the sections by a flexible tube aligned with the section central axis. The McKibben actuators are arrayed around the central axis with extending and contracting pairs on opposite sides. Pressurization of the actuators produces relative rotation between the base plates. Two miniature solenoid on/off valves are used for each contracting/extending actuator pair to inlet and exhaust air to and from the actuator.

The first section (See Fig. 2) has eight actuators connected between 3.2 mm thick aluminum base plates and is 24.1 mm long including the valves. Four of the actuators have small wind angles and are located in a square pattern about the central axis (See Fig. 3). These muscles decrease in length or contract when pressurized. The remaining actuators have large wind angles and are located in another square pattern near the edge of the base plates. These actuators increase in length or extend when pressurized. Each contracting actuator is

0-7803-8232-3/04/$17.00 ©2004 IEEE

connected to a diametrically opposed extending actuator so that both are pressurized by one valve.

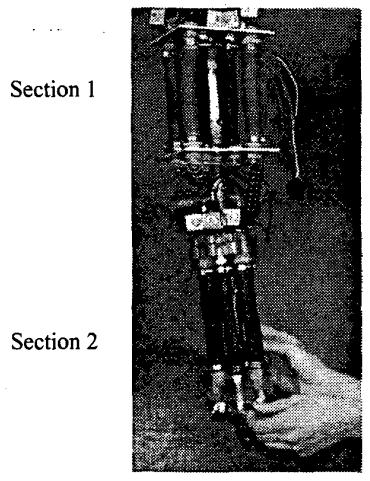

Figure 1. Artificial muscle continuum robot manipulator.

The 31.1 cm long second section has two 2.5 cm thick polycarbonate base plates connected with six McKibben Actuators arrayed in a circle about the central axis (See Figs. 2 and 3). Three of the muscles have small wind angles and are placed opposite muscles with a large wind angle. This design is mechanically simpler but more complex kinematically.

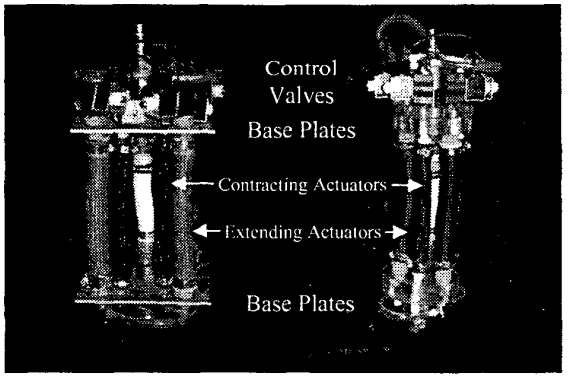

Figure 2. Section 1 (left) and section 2 of the manipulator

Solenoid valves mounted on the top base plate of each section control the flow of air into tandem pairs of actuators. Each tandem pair consists of one contracting muscle and one extending muscle with the same internal pressure and mirrored about the central axis. In this arrangement, the two muscles work together providing support for both tensile and compressive forces and stabilizing the robot to transverse loading.

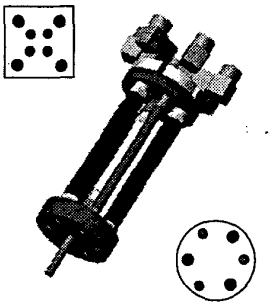

Figure 3. Actuator configuration for first (top) and second (bottom) sections (Red = contracting, Black = extending)

III. Kinematic Model

A. Section Rotation Angle

A simple model of each section provides design formulas that predict load capacity and workspace. The total arm kinematics can then be determined by combining the section results. The section response depends on an approximate McKibben actuator model [8]. If boundary and membrane effects are neglected, the actuator strain and force can be derived from the locked position with the wind angle equal to $54°44'$ (β^*). Contracting actuators under an axial load have an initial wind angle $\beta < \beta^*$ and length L at zero pressure. As the pressure increases, the wind angle increases and approaches $\beta = \beta^*$ at infinite pressure. Similarly, the extending actuators start with $\beta > \beta^*$ and converge to $\beta = \beta^*$ at infinite pressure. Thus, the maximum strain can be calculated from the locked, infinite pressure solution.

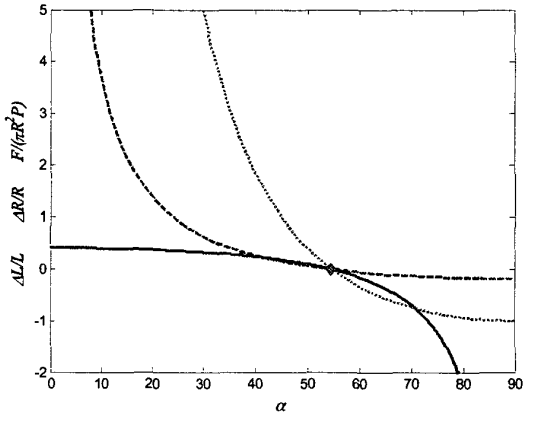

Figure 4. Nondimensionalized McKibben actuator strain ($\Delta L/L$ - solid), radius ($\Delta R/R$ - dashed), and force ($F/(\pi R^2 P)$ – dotted).

The locked solutions are only valid for large length to diameter ratio to minimize boundary effects. The available internal pressure is assumed large enough to overcome membrane effects and loading to ensure wind angles approach β^* [8].

The change in length ΔL^* starting from an initial wind angle $\beta = \alpha$ and pressurizing the actuator until $\beta = \beta^*$ is

$$\Delta L^* = \left(1 - \frac{\cos\beta^*}{\cos\alpha}\right) L. \tag{1}$$

Figure 4 shows the actuator strain versus wind angle. The maximum contractile strain is *42.3%* at $\alpha = 0$. The extensile strain has no lower bound but is practically limited by the maximum strain of the flexible tube. The maximum radial expansion of the actuators can also be estimated from locked solutions. Placing muscles too close to the central tube or other muscles can limit actuator expansion and reduce muscle strain. Based or the locked solution and the initial muscle radius R, the change in radius is

$$\Delta R^* = \left(\frac{\sin\beta^*}{\sin\alpha} - 1\right) R. \tag{2}$$

Therefore, McKibben actuators require at least $R + \Delta R^*$ in radial space to ensure maximum strain. Figure 4 shows unbounded radial expansion for small α but radial contraction limited to 18% at $\alpha = 90$ deg. The radial and longitudinal strain are zero (locked) at $\beta = \beta^*$.

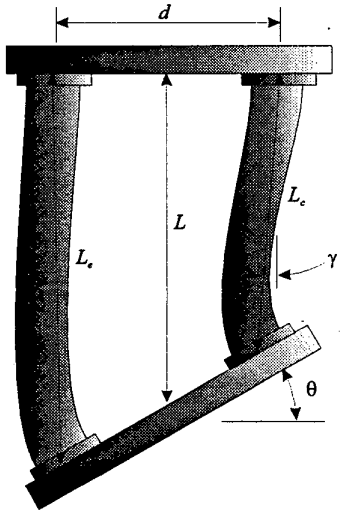

Figure 5. Section kinematic model.

The maneuverability and workspace of the manipulator section is governed by the relative motion between the supporting base plates. Figure 5 shows the base plate bending angle θ resulting from simultaneous extension and contraction of a pair of opposing actuators. The centroidal distance L is assumed constant and the bottom base plate is constrained to rotate without translation. Neglecting bending effects, the length L_c of the contracting muscle in Fig. 4 is approximately $L - \Delta L_c^*$. Considering the geometry of the right side of Fig. 4,

$$\begin{aligned} \left(L - \Delta L_c^*\right)\sin\gamma + \frac{d}{2}\left(\cos\theta - 1\right) &= 0 \\ \frac{d}{2}\sin\theta + \left(L - \Delta L_c^*\right)\cos\gamma - L &= 0 \end{aligned} \tag{3}$$

Given ΔL_c^* from Eq. (1), Eqs. (3) can be solved numerically for muscle bending angle γ and section bending angle θ. Figure 6 shows the theoretical results for three d/L ratios. As the width increases or length decreases, the maximum rotation angle decreases. Thus, long and thin arm sections will produce the most bending. Above a certain value of strain, the kinematic model no longer has a solution because the distance between the pivot point and the plate is fixed so the muscle length

$$L_c > \sqrt{L^2 + \frac{d^2}{4}}. \tag{4}$$

These limiting points are shown with circles in Fig. 6.

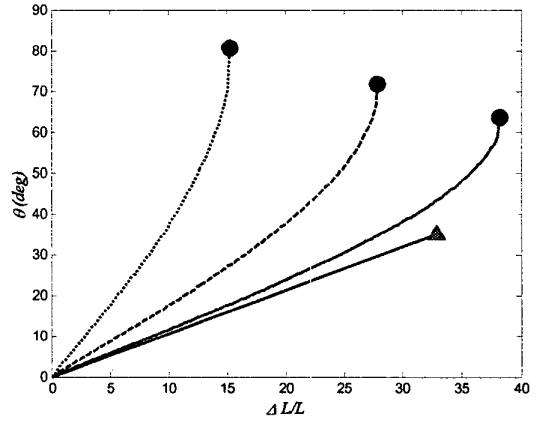

Figure 6. Experimental (solid - triangle) and theoretical (solid $d/L = 0.33$, dashed $d/L = 0.66$, and dotted $d/L = 1.0$ – circle) base plate rotation versus actuator strain (%).

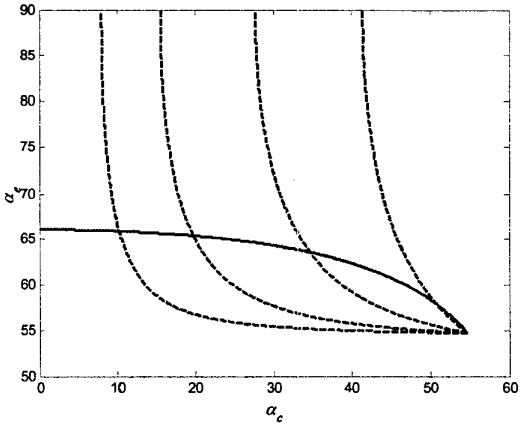

Figure 7. Matched wind angles for rotation (solid) and torque (dashed – $R_e/R_e = 0.1, 0.2, .4$, and 0.8 left to right).

Similarly, the extending muscle length $L_e = L - \Delta L_e^*$ and we can derive a set of equations like Eq. (3) for the left side of Fig. 4. For small rotation angles, these equations simplify and to ensure that the base plate has maximal rotation, $\Delta L_c^* = \Delta L_e^*$ so from Eq. (1),

$$\alpha_e = \cos^{-1}\left(\frac{\cos\beta^* \cos\alpha_c}{2\cos\alpha_c - \cos\beta^*}\right) \quad (5)$$

for matched wind angles. Figure 7 shows that to match rotation of the extending and contracting actuators, the extending actuator initial wind angle varies from 66 degrees to β^* as the contracting actuator initial wind angle varies from 0 to β^*.

B. *Load Capacity*

Muscle wind angle also influences the muscle force and manipulator load capacity. From [8], neglecting boundary (assume cylindrical muscle) and membrane (assume fiber stresses dominate) effects, if the pressure is balanced to maintain the initial muscle shape, then the muscle force

$$F = \pi R^2 P\left(2\cot^2\alpha - 1\right) \quad (6)$$

where P is the internal pressure. Figure 4 shows the actuator force in tension and compression for small and large wind angles, respectively. The compressive force is limited by the pressure acting over the actuator area $F = \pi R^2 P$ but the tension force is limited only by the strength of the tube and braided mesh.

To achieve a force balance between the contracting and extending actuators, $F_c = -F_e$ and from Eq. (6)

$$\alpha_e = \cot^{-1}\left[\sqrt{\frac{1}{2} - \frac{R_c^2}{2R_e^2}\left(2\cot^2\alpha_c - 1\right)}\right] \quad (7)$$

Thus, one can chose the muscle radius ratio R_c/R_e and wind angles to match both the forces using Eq. (7) and the rotation angle using Eq. (5). Figure 7 shows that a matched force wind angle solution does not always exist. The radicand in Eq. (7) must be positive. The tension force generated by the contracting actuator greatly exceeds the compression force generated by the extending actuator. Thus, the extending actuator diameter must be much larger than the contracting actuator to balance forces. The figure also shows that solutions exist that balance both the forces and displacements indicated by the intersections of the solid and dashed curves.

TABLE I. MANIPULATOR PARAMETERS

Section	Parameters					
1	R_c = 0.63 cm	R_e= 9.5 cm	L = 17.2 cm	d = 12.7 cm	α_c = 35 deg	α_e = 75 deg
2	R_c = 0.63 cm	R_e= 9.5 cm	L = 17.2 cm	d = 8.9 cm	α_c = 35 deg	α_e = 75 deg

IV. RESULTS AND DISCUSSION

The parameters for the experimental manipulator are shown in Table 1. The muscles for each section are constructed using latex tubing and braided polyester mesh sleeving with the contracting actuators having a smaller diameter. The initial wind angles are 35 degrees and 75 degrees for the contracting and extending actuators, respectively. From Fig. 4, the contracting actuators should provide approximately 30% contraction with a 42% change in diameter while providing 1.6 kN of force at 60 psi. The extending actuators should provide roughly 123% extension with a 15% reduction in radius and 440 N at 60 psi.

The calculated extension far exceeds the contraction so displacement matching is not achieved. In Section 1, however, the extensors are located at a larger radius than the contractors, reducing this effect. The forces are also unbalanced with the larger radius of the extensors helping to minimize this effect.

Figure 8 shows the manipulator in two poses. The antagonistically activated muscles are pressurized but show some buckling behaviour due to the unmatched displacements. With two sections, the arm can perform complicated bending.

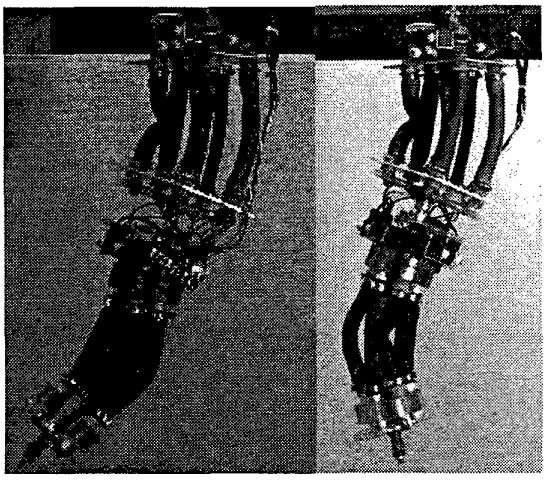

Figure 8. Manipulator in two positions.

Figure 6 shows the experimental base plate rotation comes close to the theoretically predicted value. The experimental manipulator achieved bending angles of 30 and 35 degrees for the first and second sections, respectively, at 60 psi. This is below the theoretically predicted value for several reasons. First, the actuators were not fully locked at 60 psi so their contraction/extension was not as large as predicted by Fig. 4. Second, actuator buckling reduced the effective contraction and extension. These problems could be reduced with higher pressure and more closely matched contracting and extending actuators. Finally, the base plates clearly translate as well as rotate relative to each other as seen in Fig. 8. The kinematic model does not predict this translational motion.

Figure 9 shows the manipulator lifting a weight to quantify load capacity. The equivalent nondimensional muscle force $F/(\pi R^2 P)$ was calculated from these experiments and gave

maximum values of 0.5, much less than the 3.1 predicted by the theoretical model. The maximum experimental load, however, is limited by failure of the worm gear clamps.

V. CONCLUSIONS

A novel design of a continuum manipulator using McKibben actuators is presented that is flexible between the rigid base plates. The design uses matched opposing contracting and extending McKibben actuators to produce large rotation (30 – 35 degrees per section and 50 degrees for the entire manipulator) and large load capacity (25 lb vertical lift). The manipulator has a large strength to weight ratio, high flexibility, and is simple and low cost to manufacture.

REFERENCES

[1] R. Cieslak and A. Morecki, "Elephant Trunk Type Elastic Manipulator – a Tool for Bulk and Liquid Materials Transportation," Robotica, Vol. 17 pp. 11-16, 1999.

[2] W. M. Kier and K. K. Smith, "Tongues, Tentacles, and Trunks: The Biomechanics of Movement in Muscular-hydrostats", Zoological Journal of the Linnean Society, Vol. 83, pp. 307-324, 1985.

[3] G. Klute, J. Czerniecki and B. Blacke, "McKibben Artificial Muscles: Pneumatic Actuators with Biomechanical Intelligence", IEEE International Conference on Advanced Intelligent Mechatronics, Atlanta, GA, Sept. 19-22, pp 1-5, 1999.

[4] G. Robinson and J.B.C. Davies, "Continuum Robots – A State of the Art," IEEE Int. Conf. on Robotics and Automation, Detroit, MI, pp. 2849-2853, May 1999.

[5] J. F. Wilson, D. Li, Z. Chen and R.T. George, Jr., "Flexible Robot Manipulators and Grippers: Relatives of Elephant Trunks and Squid Tentacles", Duke University, Durham, N.C, pp. 475-494.

[6] J.L. Van Leeuwan, J.L. and W. M. Kier, "Functional Design of Tentacles in Squid: Linking Sarcomere Ultrastructure to Gross Morphological Dynamics", Phil. Trans. Royal Society. London B, 1997, pp. 1-21

[7] R.S. McCurley and W. M. Kier, "The Functional Morphology of Starfish Tube Feet: the Role of a Crossed-Fiber Helical Array in Movement." Biol. Bull., Vol. 188, pp. 197-209, Apr. 1995.

[8] Liu, W., and Rahn, C., "Fiber Reinforced Membrane Models of McKibben Actuators," ASME Journal of Applied Mechanics, Vol. 70, No. 6, pp. 853-859, November 2003.

[9] Li, C., and Rahn, C., "Design of Continuous Backbone, Cable-Driven Robots," ASME Journal of Mechanical Design, Vol. 124, No. 2, pp. 265 - 271, June 2002.

[10] Gravagne, I., Rahn, C., and Walker, I., "Large Deflection Dynamics and Control for Planar Continuum Robots," IEEE/ASME Transactions on Mechatronics, Vol. 8, No. 2, pp. 299 – 307, June 2003.

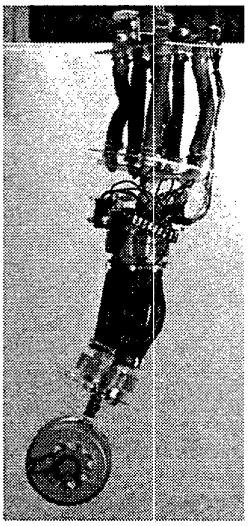

Figure 9. Manipulator lifting weight.